Published in final edited form as:

J Biomed Mater Res A. 2021 January ; 109(1): 6–17. doi:10.1002/jbm.a.37002.

3D Bioprinting of Oligo(Poly(Ethylene Glycol) Fumarate) for Bone and Nerve Tissue Engineering

Xifeng Liu[a,b], **Bipin Gaihre**[a,b], **Matthew N. George**[a,b], **A. Lee Miller II**[b], **Haocheng Xu**[a,b], **Brian E. Waletzki**[b], **Lichun Lu**[*,a,b]

[a]Department of Physiology and Biomedical Engineering, Mayo Clinic, Rochester, MN 55905, USA

[b]Department of Orthopedic Surgery, Mayo Clinic, Rochester, MN 55905, USA.

Abstract

3D bioprinting is a promising new tissue restoration technique that enables the precise deposition of cells and growth factors in order to more closely mimic the structure and function of native organs. In this study, we report the development of a new bioink using oligo(poly(ethylene glycol) fumarate) (OPF), a photo-crosslinkable and biodegradable polymer, for 3D bioprinting. In addition to OPF, a small portion of gelatin was also incorporated into the bioink with to make it bio-printable. After immersion in the cell medium, gelatin was eluted away to create a bioprinted scaffold of pure OPF. Excellent cell viability, spreading, and long-term proliferation of encapsulated cells was observed using both bone and nerve cells as examples. These results demonstrate that OPF bioink has great potential in future 3D bioprinting applications that aim to replicate complex, layered tissues and/or organs.

Keywords

3D bioprinting; bioink; oligo(poly(ethylene glycol) fumarate); tissue engineering; hydrogel

1. Introduction

The 3D printing of biological materials, commonly named 3D bioprinting, provides a promising substitute for future tissue and organ restoration by combining engineering techniques and biological principles into one system.[1–3] The biggest advantage of 3D bioprinting is that it allows biomaterials, cells, growth factors, and other bioactive cues to be precisely deposited in three-dimensional space, allowing for the close replication of the complex architecture that is commonly found in native organs.[4–6] Due to this advantage, 3D bioprinting has gained extensive attention from many fields including biomedical engineering, tissue engineering, organ engineering, regenerative medicine, and cancer treatment.[7–14] With intensified research efforts, 3D bioprinting has received rapid technological development in instruments, biological inks, crosslinking methods, and printing models in recent years.[3,15–18]

[*]Corresponding Author: Lu.Lichun@mayo.edu. Tel.: 507-284-2267. Fax: 507-284-5075.

Conflict of Interests

The authors declare no competing financial interest.

The most widely used 3D bioprinting modalities are inkjet bioprinting/droplet bioprinting, laser-assisted bioprinting, and extrusion-based bioprinting.[19–22] However, regardless of the technique used, the technical bottleneck in these bioprinting systems is not due to the printing technology itself but instead lies in the ideal formulation of bioink materials.[23,24] An ideal bioink should combine numerous properties together into one formulation. These properties include but are not limited to, 1) a favorable viscosity to prevent blocking the print head, 2) a quick shear recovery rate to facilitate the immediate cessation of flow upon deposition, 3) the ability to form covalent or ionic bonds among polymer chains (crosslink) to maintain a printed shape after deposition, 4) good biocompatibility to maintain viable cells, and 5) biodegradability to leave all space for tissue/organ formation.[25–29]

Hydrogels, which are thoroughly hydrated polymers, proteins, or peptide networks that able to retain large quantities of water,[30,31] are one of the most favorable biomaterials used for 3D bioprinting.[16] Various natural or synthetic polymer was tried as bioinks for tissue engineering, including alginate-based gels, gelatin methacryloyl (GelMA) gels, and poly(ethylene glycol (PEG) gels.[27] Oligo(poly(ethylene glycol) fumarate) (OPF) is a biocompatible polymer made up of hydrophilic poly(ethylene glycol) (PEG) chains adorned with double bonds that, when irradiated with ultraviolet radiation (UV), open and crosslink with each other to form a soft hydrogel.[32,33] The resulting crosslinked OPF hydrogel is biodegradable *in situ* through the hydrolysis of ester bonds,[34] while also displaying impressive biocompatibility in both *in vitro* and *in vivo* studies investigating bone and nerve tissue regeneration.[35–38]

In this study, we report the development of an OPF-based bioink for tissue engineering (Fig. 1a). The bioink consisted of a crosslinkable OPF polymer with a small portion of gelatin. Prior to bioprinting, cells were first encapsulated within a sterilized OPF/gelatin solution, resulting in a cell/ink slurry. This slurry was then quickly cooled to obtain a viscous bioink gel taking advantage of the sol-gel transition of gelatin chains formed within the bioink (Fig. 1b). The bioink was then printed using a gas-assisted extrusion bioprinter to form the desired shape, inducing polymer crosslinking through UV light exposure to form a stabilized hydrogel with cells encapsulated within (Fig. 1c). The bioprinted scaffold was finally washed with pre-warmed cell culture medium to dissolve and elute the gelatin portion (Fig. 1c).

2. Materials and Methods

2.1 Polymer Synthesis

OPF was synthesized in accordance with our previous reports.[39–41] In brief, 100 g of PEG with a nominal number average molecular weight (M_n) of 10,000 g mol^{-1} was added into a three-neck flask purged with nitrogen gas. Then 800 mL CH_2Cl_2 (dichloromethane, DCM) solvent was added and stirred for 30 min to allow the full dissolution of the PEG polymer. Excess K_2CO_3 (40 g) was added as a proton scavenger for the following reaction (Fig. 2a). The flask with PEG/DCM/K_2CO_3 was then placed into an ice bath and 1.1 mL of fumaryl chloride was added dropwise. The system was kept stirring at a 50°C for 24 hours under reflux. To remove unreacted K_2CO_3 particles, the mixture was transferred into a 50 mL falcon tube and centrifuged at 3000 rpm for 10 min. The supernatant was collected and

the synthesized OPF polymer was precipitated in diethyl ether and dried overnight under vacuum. The structure of synthesized OPF was confirmed by ^{1}H nuclear magnetic resonance (NMR) using deuterated chloroform ($CDCl_3$) as the solvent.

2.2 Bioink Evaluation

Crosslinkability, gelation, and printability.—A series of inks with varied OPF concentrations of 5, 10, 15, 20, and 25 wt% and gelatin percentages of 1, 2, 3, 4, 5, 6, 7, 8, 9, 10 wt% relative to the α-Minimum Essential Medium (α-MEM) volume were fabricated. The crosslinkability of bioinks was checked after UV irradiation for 2 minutes. After immersing in deionized (DI) water overnight, the gels that maintained a cohesive shape were marked as good. Others that had big cracks or broken into large pieces after a soak in water overnight were marked as fair. Bioinks that broken into many small pieces in water were marked poor crosslinkability.

The gelation ability of bioink formulations after kept stable on table for 24 hours (~18–20 °C) was examined using the tube inversion method, as referred to previous reports.[42] After inversion, the bioinks that created full and homogeneous gels were recorded as good. The ones with at least half gel formation were recorded as fair. Those with less than half gel formations were recorded as poor gelation.

The printability of these inks using a 0.25 mm diameter print head on a Bio-X bioprinter (CELLINK, Gothenburg, Sweden) under a pressure range of 1–100 kPa was also investigated and recorded. The goal shape of scaffolds is 10 mm × 10 mm width and length, and 1 layer of 0.25 mm thickness, with 25% infill density. The bioinks that could be printed into uniform and continuous shapes were recorded as good. The bioinks that could be printed to shapes, however, unperfect or non-uniform, were recorded as fair. All other situations where the inks formed non-continuous or incomplete shapes were recorded as poor.

Scanning electron microscopy (SEM).—Hydrogel samples were all dried by lyophilization for 3 days. Dried samples were immersed in liquid nitrogen for 1 min to freeze the structure and then broken open using forceps. The exposed broken surfaces were sputter-coated with gold-palladium and examined on a scanning electron microscope (S-4700, Hitachi Instruments, Tokyo, Japan) at 5 kV voltage.

Cytotoxicity of leaching medium.—To evaluate whether the bioinks could release cytotoxic substances to the surrounding cells, the crosslinked hydrogel specimens were placed into transwell chambers (mesh size 3 μm). MC3T3-E1 pre-osteoblast cells were seeded into six-well TCPS plates seeded at a density of 15,000 cells per well and cultured using α-MEM media supplemented with 0.5% streptomycin/penicillin and 10% fetal bovine serum. Cells were placed in a 37 °C cell culture hood for 6 hours to allow attachment to the bottom of the plate. Then the transwell chambers with hydrogel specimens were inserted into the six-well plates and the plates were placed back into 37 °C cell culture hood. Wells without sample treatment was used as a positive control. At 1, 3, and 7 days co-culture, the cell density in each well was determined with the MTS assay (CellTiter 96, Promega, Madison, WI), reading absorbance on a UV-vis absorbance microplate reader (SpectraMax

Plus 384, Molecular Devices, Sunnyvale, CA) at a wavelength of 490 nm. Cell viability in each well was calculated by normalizing absorbance to that of the positive control wells (set as 100%).

2.3 Bioprinting

Gel preparation.—To prepare the gelated formulation, 15 wt% of OPF polymer and 5 wt% gelatin were added to 1 mL of α-MEM, with 30 μL of polyethylene glycol diacrylate (PEGDA, M_n ~ 570 g/mol) added as a crosslinker, and 2.5 mg of Irgacure 2959 (Sigma-Aldrich Co., Milwaukee, WI) added as photo-initiator. The mixture was then kept at 60°C for 30 min while protected from light to allow the full dissolution of OPF polymer and gelatin. The dissolved mixture was then sterilized by filtering through a 0.45 μm sterile syringe filter (Whatman, GE Healthcare Bio-Sciences, Pittsburgh, PA), as previously reported.[43] The filtered stock solution was kept at 4°C for 1 hour to allow gelation and subsequently stored at 4°C before usage.

Cell collection.—MC3T3 pre-osteoblast cells for bioprinting were first expanded in big 150 × 25 mm tissue culture dishes (Becton Dickenson, Franklin Lakes, NJ) using α-MEM supplemented with 0.5% streptomycin/penicillin and 10% fetal bovine serum. After reaching ~ 80% confluency, the cells were trypsinized and counted. Cell suspensions with desired cell numbers were centrifuged at 3000 rpm for 10 min and the supernatant was removed gently to collect cells.

Bioink preparation.—To prepare bioink, the gelled mixture was taken out of the 4°C fridge and re-liquidized in a 37°C water bath. The melted gel was then added with the collected cells and gently mixed under sterile conditions. The cell/gel mixture was then placed on ice for 1 min to obtain the gelled bioink.

Bioprinting and crosslinking.—The bioink with encapsulated cells was printed using a 0.25 mm diameter print head on a Bio-X bioprinter (CELLINK, Gothenburg, Sweden). Following bioprinting, scaffolds were immediately exposed to UV light for 2 min to allow crosslinking. The crosslinked, bioprinted scaffolds were washed with prewarmed 37°C α-MEM three times, and immersed in excess α-MEM and cultured in a 37°C cell culture incubator.

2.5. Immediate Cell Viability after Bioprinting

To investigate the immediate cell viability after bioprinting, MC3T3 pre-osteoblast cells were bioprinted at a density of 1×10^6 cells/mL of bioink. Immediately after bioprinting, gels were cross-linked through UV exposure for 2 minutes and cells were stained using the LIVE/DEAD® Cell Imaging Kit (Thermo Fisher Scientific, Waltham, MA). The live cells (green) and dead cells (red) embedded within the bioprinted scaffolds were viewed using an inverted laser scanning confocal microscope (LSM 780, Carl Zeiss, Germany). The morphological properties of the printed scaffolds were observed using an Axiovert 25 Zeiss light microscope (Carl Zeiss, Germany).

2.6 Bone Cell Proliferation

To investigate the long-term cell viability and proliferation in the bioprinted hydrogel, MC3T3 pre-osteoblast cells were bioprinted at a density of 10×10^6 cells/mL of bioink. The shape of the scaffolds printed is 10 mm × 10 mm width and length, and 1 layer of 0.1 mm thickness. After bioprinting, scaffolds were immediately exposed to UV light for 2 min for photo-crosslinking. Scaffolds with cells encapsulated within were washed 3 times with excess pre-warmed α-MEM to dissolve and wash away the gelatin coils. The cell/scaffold constructs were then cultured in α-MEM at 37°C. At 1, 4, and 7 days post-seeding, the constructs were stained with LIVE/DEAD® Cell Imaging Kit and viewed with an inverted laser scanning confocal microscope as described above. The MC3T3 pre-osteoblast cell densities proliferated in the bioinks were determined using the MTS assay (CellTiter 96, Promega, Madison, WI). The optical absorbances were read on a UV-vis absorbance microplate reader (SpectraMax Plus 384, Molecular Devices, Sunnyvale, CA) with wavelength at 490 nm. Average values and statistical analyses were calculated on four independent tests.

2.7 Nerve Cell Proliferation

PC12 neuronal cells were purchased from American Type Culture Collection (ATCC) and expanded in big 150 × 25 mm tissue culture dishes using Dulbecco's Modified Eagle Medium (DMEM) supplemented with 5% fetal bovine serum, 10% horse serum, and 0.5% streptomycin/penicillin, and incubated at 37 °C with a 95% relative humidity and 5% CO_2. After reaching 80% confluency, PC12 cells were trypsinized and centrifuged at 3000 rpm for 10 min and mixed into bioink at a density of 10×10^6 cells/mL using the same procedure as described in the MC3T3 cell mixing section. After bioprinting, scaffolds were immediately exposed to UV light for 2 min for photocrosslinking. Crosslinked scaffolds were then washed 3 times with excess pre-warmed DMEM to elute the gelatin coils and the cell/scaffold constructs were cultured in DMEM in a 37 °C incubator. After 1, 4, and 7 days of culture, the constructs were stained with LIVE/DEAD® Cell Imaging Kit and viewed with an inverted laser scanning confocal microscope as described above. The PC12 cell densities proliferated in the bioinks were determined using the MTS assay and read on a UV-vis absorbance microplate reader at 490 nm, as described above. Average values and statistical analyses were calculated on four independent tests.

2.8 Statistical analysis

The statistical difference among varied experimental groups was analyzed using a one-way analysis of variance (ANOVA) with post hoc Tukey HSD test when necessary. Any two data groups with p-value calculated lower than 0.05 were marked with a significant difference.

3. Results

3.1 Bioprinting Setup and Bioink Screen

OPF was successfully synthesized and the structure was confirmed by ^1H nuclear magnetic resonance (NMR) using deuterated chloroform ($CDCl_3$) as solvent (Fig. 2a–b). To determine the bioprintability and cell viabilities in printed scaffolds, MC3T3 pre-osteoblast cells were

collected by centrifugation and mixed with OPF/Gelatin slurry (1×10^6 cells/mL) to make bioinks, as presented in Fig. 3a. The bioinks were then printed using a CELLINK Bio-X printer setup (Fig. 3b) followed by UV crosslinking for 2 min.

For bioinks to be useful in tissue engineering applications, the crosslinkability, gelation ability, and printability of the bioink formulations must be optimized to meet the challenges of 3D printing as well as *in vivo* implantation. In order to screen the best bioink, we fabricated a series of inks with varied OPF concentrations and gelatin percentages. As demonstrated in Fig. 3c, the crosslinking ability of inks was enhanced by the addition of OPF but inhibited by the presence of gelatin. A higher OPF concentration aided in the crosslinking process, while a higher gelatin concentration interfered with successful crosslinking, particularly when the gelatin portion was higher than 6% and the OPF concentration was lower than 10%.

In addition to crosslinking ability, the gelation capability of a bioink is also critical. Gelation in OPF/Gelatin originated from the formation of coils among gelatin polymer chains. As can be noted in Fig. 3d, better gelation observed as the gelatin percentage increased. When OPF is 5% in the formulation, good gelation was observed with the addition of ≥ 2% gelatin. When OPF increased to 10 and 15%, good gelation was observed with ≥ 4% gelatin. When OPF increased to 20 and 25%, gelation was observed only with higher gelatin fractions of ≥ 7% or even 9%.

The printability of the bioinks was also investigated. Results showed that printability is closely related to gelation. For inks with less than 3% gelatin, gelation was not successfully achieved and the ink was similar to free-fluid, leading to poor printability. For inks with more than 3% gelatin, gelation occurred and the inks were able to be printed into different shapes by adjusting the printing parameters (Fig. 3e). However, inks with extremely high gelatin concentration (9–10%) yet low OPF content (5–10%), the printability performance was also inadequate. This result may be due to the high stiffness of inks at high concentrations of gelatin, preventing effective and continuous extrusion of the material from the printing head (Fig. 3e). Based on these results, a bioink with 15 wt% OPF and 5 wt% gelatin was selected for further bioprinting analysis.

Cell viability within gels was determined immediately after bioprinting and crosslinking using LIVE/DEAD staining. Live and dead cells were counted and the proportion of each was obtained by dividing by total cell number. For bioinks with weak crosslinkability or printability, the obtained shapes were not perfect and cells were counted from the imperfect pieces. As shown in Fig. 3f, when OPF content is as high as 20–25% in the bioink, cell viability dropped drastically. However, bioinks with OPF content lower than 15% showed most of the cells were alive with only a small portion of dead cells likely caused by the extrusion pressure. An enlarged view of the live/dead cell imaging in 15% OPF and 5% gelatin showed potential live cells within the bioink (Fig. 3g). These results indicate that cell viability is closely related to the ratio of components within the ink. This result is consistent with previous reports that display robust cell viabilities using hydrogels as bioinks.[44–46]

3.2 Bioprinted scaffold properties

Based on the above bioink screen results, the bioink with 15 wt% OPF and 5 wt% gelatin in cell medium has the favorable crosslinking ability, gelation, printability, and relatively high cell viability, thus was selected for bioprinting of scaffolds. Various infill densities could be achieved by adjusting the printing parameters, with example photographs shown in Fig. 4a. Bioprinted scaffolds were examined under a microscope to determine the shape integrity and continuity, as well as cell distribution. As can be seen from Fig. 4b, scaffolds showed homogeneous ridges and cross-sections. Cells were also observed to distribute homogeneously across the scaffolds, as noted from the enlarged view of these scaffolds (Fig. 4c).

In addition to rectangular scaffolds, bioinks can also be printed into round shapes with circular edges. A typical photograph of the bioprinted round scaffolds was presented in Fig. 4d. The microscopic images showed that round scaffolds also had homogeneous cell distribution and shape integrity and continuity, even at the edges (Fig. 4e).

To evaluate the properties of the bioink, crosslinked OPF ink before and after washing were fabricated into round shaped disks for gel properties evaluation. After lyophilization, the micro-structures within the hydrogel were observed by SEM. As presented in Fig. 5a–b, gels after washing showed porous structures within the hydrogel as compared with gels before washing. This indicates that the gelatin can be washed away and leave microporous structures within the gel. To evaluate whether the crosslinked OPF bioink gel produces byproducts that are cytotoxic to the surrounding cells, hydrogels were placed into transwells and cocultured with MC3T3 cells for 1, 3, and 7 days. As shown in Fig. 5c, no significant cytotoxicity was observed for the bioink after coculturing with cells.

3.3 Bioprinting and proliferation of bone cells

The cell viability and densities of MC3T3 pre-osteoblast cells in bioprinted scaffolds were investigated after culturing for 1, 4 and 7 days. As observed by confocal imaging in Fig. 6a, the bioprinted cells were homogeneously distributed within the bioprinted scaffolds and showed a round shape after 1-day in culture. After 4 days, cell growth was observed to start on the edge of the bioscaffolds, which may be because cells at these locations were exposed to an abundance of oxygen and nutrients (Fig. 6b). After 7 days of culture, cell growth was observed on the edge of the bioscaffolds as well as within bioscaffolds (Fig. 6c).

A specific analysis of typical cell morphologies was further conducted. At day 1, cells showed mainly round shape with limited filament outgrowth, as depicted by the schematic demonstration of each cell (Fig. 6d). However, after 4 days of culture, cells in the bioprinted scaffolds showed elongated shape with filament outgrowth (Fig. 6e). An enlarged view of typical cells showed clear filament outgrowth, as illustrated in the schematic demonstration. After 7 days of culture, a large population of cells was observed and cells were directly in contact with one another, indicating that intercellular interactions were achieved between encapsulated cells (Fig. 6f). These results indicate that bioprinted scaffolds could allow nutrient penetration and support good cell growth within the scaffolds. The MC3T3 pre-osteoblast cells were quantified to be mostly alive in the scaffolds, as shown in Fig. 6g.

The proliferation study showed significant cell growth after 7 days of culture (Fig. 6h). This observation is consistent with other reports describing cell proliferation during 1 week of culture after bioprinting.[47]

3.4 Bioprinting and proliferation of nerve cells

In addition to pre-osteoblasts, the viability and growth of PC12 nerve cells were also investigated. As presented in Fig. 7a, PC12 cells showed excellent viability within the bioprinted scaffolds after 1, 4 and 7 days' culture. Similar to MC3T3 pre-osteoblasts, PC12 cells also showed round-shaped morphology at day 1 of culture (Fig. 7a–b), indicating that OPF bioink was also biocompatible with PC12 nerve cells. After 4 and 7 days of culture, proliferated cell groups were observed by confocal imaging (Fig. 7c–f). 3D reconstruction of confocal images taken at randomly chosen areas in the bioink showed that the cells proliferated both at the edges and within the bioprinted scaffolds (Fig. 7c–f). The PC12 nerve cells were also determined to be mostly alive in the scaffolds (Fig. 7g). The proliferation of cells was also observed, with significantly larger numbers of cells after 4 and 7 days of culture (Fig. 7h). These results demonstrated that OPF bioink could support the excellent proliferation of PC12 nerve cells.

Discussions

OPF based hydrogels have received significant attention due to their use as cellular scaffolds for cartilage, bone, and nerve tissue regeneration applications.[33,35,37,48] A versatile system, the presence of reactive fumarate double bonds makes OPF cross-linkable using either a chemical or photo-crosslinking strategy, while the frequent ester bond repeats throughout the network facilitate non-toxic biodegradation. Several studies have successfully demonstrated that crosslinked OPF hydrogels are able to encapsulate the cells with minimal effect on their metabolic activities.[48,49] Furthermore, with certain biological cues, the encapsulated cells have been shown to differentiate into the desired phenotype.[50] These findings motivated the current study wherein 3-D bioprinted OPF hydrogels with encapsulated-cells have been developed. Here, we have proposed OPF-Gelatin as a bioink for further bioprinting applications.

Bioprinting techniques enable the spatial patterning of cells and other biological factors within the polymer matrix,[51] improving the timely and precise development of the functional tissues. Hydrogel-based bioinks display a number of attractive properties that support this application, motivating the development of a number printable hydrogels that incorporate biological and synthetic compounds including gelatin methacryloyl (GelMA), polyethylene glycol diacrylate (PEGDA), alginate, collagen, hyaluronic acid (HA), chitosan, Pluronic, fibrin/fibrinogen, silk, agarose, and blends of these materials.[27,28,52,53] Extrusion based bioprinting is one of the most commonly applied printing technique. It provides superior control over the cell deposition and distribution.[51] One of the well-acknowledged limitations of extrusion-bioprinting is the high possibility of cell apoptosis due to the pressure exerted on the cells during extrusion through micro-nozzle. To ameliorate this concern, the optimization of bioprinting parameters including material amount, applied pressure, and temperature is vital for successful extrusion-bioprinting.[54]

In this study, we successfully demonstrated OPF hydrogels can be developed into a bioink for extrusion-based 3-D bioprinting. In its native form, the viscosity of the OPF solution does not support extrusion-based printing. However, through the addition of a gelatin fraction that doubles as a porogen after hydrogel crosslinking, our results show that OPF bioinks can support uniform extrusion when the gelatin content is optimized. The gelatin was added into OPF bioink formulations for two disparate reasons. First, during the bioprinting process, the OPF itself is not bioprintable without the addition of high viscous components. The inclusion of gelatin provides favorable rheological properties to the bioink, facilitating the extrusion of the ink and the structural integrity of the printed structure (Fig. 1a). Second, after a 3D structure has been printed, gelatin can be eluted away through immersion in warm cell medium, leaving porous structures within the hydrogel. These two steps are based on the reversible gelation nature of the gelatin chains (Fig. 1b). The gelatin solution exists as a liquid form at 37 °C but can transform into a soft viscous gel at a gelling temperature ($T_{Gel,}$ close to room temperature ~21 °C) or even below.[55,56] This transition is realized by the formation of coil-helix with intermolecular bonds. This unique material property is reversible when temperatures are increased above the T_{Gel} threshold, resulting in the destruction of gelatin coils solubilization of the gel network.

At gelatin concentrations higher than 9% or lower than 3%, impaired printing was observed. Our overall optimization work on gelation and extrusion showed that the bioink with 15 wt% OPF and 5% gelatin was well suited for the printing. Furthermore, this composition was found to support the viability of encapsulated MC3T3-E1 and PC12 cells. The encapsulated cells not only maintained excellent viability but also showed a good proliferation over a seven-day period. The porosity created by the eroding gelatin enabled the rapid and continuous diffusion of nutrients into the hydrogel which might have contributed to the excellent cell response. Furthermore, gelatin itself has cell-binding sites which can positively influence the cell attachment and proliferation.[57] Future studies will be focused on exploring more on printing multiple cell types and incorporating suitable biological cues for functional bone and nerve tissue regeneration.

Conclusions

In summary, we developed a ‘micro-structured’ hydrogel bioink with a network of pores designed to enhance the flux of oxygen and nutrients to encapsulated cells. Using a crosslinkable, biodegradable OPF polymer as the polymer backbone and gelatin as a porogen, a series of bioinks with various compositions were fabricated, and their crosslinkability, gelation ability, and printability were evaluated. Following bioprinting, scaffolds were washed with cell culture medium to remove gelatin from the crosslinked network and to create void volumes within the material. The OPF bioink formulations comprised of 15 wt% OPF and 5 wt% gelatin were found to display superior printability, gelation, and crosslinkability and were selected for evaluation using MC3T3 pre-osteoblast cells. Live/dead cell staining showed that the cells had good viability after bioprinting, while an excellent proliferation of cells was observed after culturing the bioprinted scaffolds in the medium for one week. In addition to pre-osteoblasts, PC12 nerve cells were also bioprinted and showed excellent cell proliferation within the scaffolds. These results demonstrate that

the OPF bioink is a promising choice for future 3D bioprinting systems aiming at tissue and organ engineering.

Acknowledgments

This work was supported by the National Institutes of Health grant R01 AR56212.

References

1. Mandrycky C, Wang Z, Kim K, Kim D-H. 3D bioprinting for engineering complex tissues. Biotechnology advances 2016;34(4):422–434. [PubMed: 26724184]
2. Kang H-W, Lee SJ, Ko IK, Kengla C, Yoo JJ, Atala A. A 3D bioprinting system to produce human-scale tissue constructs with structural integrity. Nature biotechnology 2016;34(3):312.
3. Murphy SV, Atala A. 3D bioprinting of tissues and organs. Nature biotechnology 2014;32(8):773.
4. Kolesky DB, Truby RL, Gladman AS, Busbee TA, Homan KA, Lewis JA. 3D bioprinting of vascularized, heterogeneous cell-laden tissue constructs. Advanced materials 2014;26(19):3124–3130. [PubMed: 24550124]
5. Markstedt K, Mantas A, Tournier I, Martínez Ávila Hc, Hägg D, Gatenholm P. 3D bioprinting human chondrocytes with nanocellulose–alginate bioink for cartilage tissue engineering applications. Biomacromolecules 2015;16(5):1489–1496. [PubMed: 25806996]
6. Duan B, Hockaday LA, Kang KH, Butcher JT. 3D bioprinting of heterogeneous aortic valve conduits with alginate/gelatin hydrogels. Journal of biomedical materials research Part A 2013;101(5):1255–1264. [PubMed: 23015540]
7. Albritton JL, Miller JS. 3D bioprinting: improving in vitro models of metastasis with heterogeneous tumor microenvironments. Disease models & mechanisms 2017;10(1):3–14. [PubMed: 28067628]
8. Stanton M, Samitier J, Sanchez S. Bioprinting of 3D hydrogels. Lab on a Chip 2015;15(15):3111–3115. [PubMed: 26066320]
9. Zhang YS, Yue K, Aleman J, Mollazadeh-Moghaddam K, Bakht SM, Yang J, Jia W, Dell'Erba V, Assawes P, Shin SR. 3D bioprinting for tissue and organ fabrication. Annals of biomedical engineering 2017;45(1):148–163. [PubMed: 27126775]
10. Ozbolat IT, Peng W, Ozbolat V. Application areas of 3D bioprinting. Drug discovery today 2016;21(8):1257–1271. [PubMed: 27086009]
11. Gao G, Cui X. Three-dimensional bioprinting in tissue engineering and regenerative medicine. Biotechnology letters 2016;38(2):203–211. [PubMed: 26466597]
12. Bishop ES, Mostafa S, Pakvasa M, Luu HH, Lee MJ, Wolf JM, Ameer GA, He T-C, Reid RR. 3-D bioprinting technologies in tissue engineering and regenerative medicine: Current and future trends. Genes & diseases 2017;4(4):185–195. [PubMed: 29911158]
13. Wu W, DeConinck A, Lewis JA. Omnidirectional printing of 3D microvascular networks. Advanced materials 2011;23(24):H178–H183. [PubMed: 21438034]
14. Lee VK, Kim DY, Ngo H, Lee Y, Seo L, Yoo S-S, Vincent PA, Dai G. Creating perfused functional vascular channels using 3D bio-printing technology. Biomaterials 2014;35(28):8092–8102. [PubMed: 24965886]
15. Włodarczyk-Biegun MK, del Campo A. 3D bioprinting of structural proteins. Biomaterials 2017;134:180–201. [PubMed: 28477541]
16. Hinton TJ, Jallerat Q, Palchesko RN, Park JH, Grodzicki MS, Shue H-J, Ramadan MH, Hudson AR, Feinberg AW. Three-dimensional printing of complex biological structures by freeform reversible embedding of suspended hydrogels. Science advances 2015;1(9):e1500758. [PubMed: 26601312]
17. Li J, Chen M, Fan X, Zhou H. Recent advances in bioprinting techniques: approaches, applications and future prospects. Journal of translational medicine 2016;14(1):271. [PubMed: 27645770]
18. Lee VK, Dai G. Printing of three-dimensional tissue analogs for regenerative medicine. Annals of biomedical engineering 2017;45(1):115–131. [PubMed: 27066784]

19. Wüst S, Müller R, Hofmann S. Controlled positioning of cells in biomaterials—approaches towards 3D tissue printing. Journal of functional biomaterials 2011;2(3):119–154. [PubMed: 24956301]
20. Dababneh AB, Ozbolat IT. Bioprinting technology: a current state-of-the-art review. Journal of Manufacturing Science and Engineering 2014;136(6):061016.
21. Wang Z, Abdulla R, Parker B, Samanipour R, Ghosh S, Kim K. A simple and high-resolution stereolithography-based 3D bioprinting system using visible light crosslinkable bioinks. Biofabrication 2015;7(4):045009. [PubMed: 26696527]
22. Feinberg AW, Miller JS. Progress in three-dimensional bioprinting. MRS Bulletin 2017;42(8):557–562.
23. Ozbolat IT, Yu Y. Bioprinting toward organ fabrication: challenges and future trends. IEEE Transactions on Biomedical Engineering 2013;60(3):691–699. [PubMed: 23372076]
24. Jose RR, Rodriguez MJ, Dixon TA, Omenetto F, Kaplan DL. Evolution of bioinks and additive manufacturing technologies for 3D bioprinting. ACS Biomaterials Science & Engineering 2016;2(10):1662–1678.
25. Hölzl K, Lin S, Tytgat L, Van Vlierberghe S, Gu L, Ovsianikov A. Bioink properties before, during and after 3D bioprinting. Biofabrication 2016;8(3):032002. [PubMed: 27658612]
26. Billiet T, Gevaert E, De Schryver T, Cornelissen M, Dubruel P. The 3D printing of gelatin methacrylamide cell-laden tissue-engineered constructs with high cell viability. Biomaterials 2014;35(1):49–62. [PubMed: 24112804]
27. Gungor-Ozkerim PS, Inci I, Zhang YS, Khademhosseini A, Dokmeci MR. Bioinks for 3D bioprinting: an overview. Biomaterials science 2018;6(5):915–946. [PubMed: 29492503]
28. Hospodiuk M, Dey M, Sosnoski D, Ozbolat IT. The bioink: a comprehensive review on bioprintable materials. Biotechnology advances 2017;35(2):217–239. [PubMed: 28057483]
29. Chimene D, Lennox KK, Kaunas RR, Gaharwar AK. Advanced bioinks for 3D printing: a materials science perspective. Annals of biomedical engineering 2016;44(6):2090–2102. [PubMed: 27184494]
30. Peppas NA, Hilt JZ, Khademhosseini A, Langer R. Hydrogels in biology and medicine: from molecular principles to bionanotechnology. Advanced materials 2006;18(11):1345–1360.
31. Zou Y, Zhang L, Yang L, Zhu F, Ding M, Lin F, Wang Z, Li Y. “Click” chemistry in polymeric scaffolds: Bioactive materials for tissue engineering. Journal of controlled release 2018;273:160–179. [PubMed: 29382547]
32. Liu X, Paulsen A, Giambini H, Guo J, Miller AL, Lin P-C, Yaszemski MJ, Lu L. A New Vertebral Body Replacement Strategy Using Expandable Polymeric Cages. Tissue Engineering Part A 2016;23(5–6):223–232. [PubMed: 27835935]
33. Liu X, Miller AL, Park S, Waletzki BE, Zhou Z, Terzic A, Lu L. Functionalized Carbon Nanotube and Graphene Oxide Embedded Electrically Conductive Hydrogel Synergistically Stimulates Nerve Cell Differentiation. ACS Applied Materials & Interfaces 2017;9(17):14677–14690. [PubMed: 28406608]
34. Qiu Y, Lim JJ, Scott L, Adams RC, Bui HT, Temenoff JS. PEG-based hydrogels with tunable degradation characteristics to control delivery of marrow stromal cells for tendon overuse injuries. Acta biomaterialia 2011;7(3):959–966. [PubMed: 21056127]
35. Olthof MG, Tryfonidou MA, Liu X, Pouran B, Meij BP, Dhert WJ, Yaszemski MJ, Lu L, Alblas J, Kempen DH. Phosphate Functional Groups Improve Oligo [(Polyethylene Glycol) Fumarate] Osteoconduction and BMP-2 Osteoinductive Efficacy. Tissue Engineering Part A 2018;24(9–10):819–829. [PubMed: 29065776]
36. Liu X, Fundora KA, Zhou Z, Miller AL, Lu L. Composite Hydrogel Embedded with Porous Microspheres for Long-Term pH-Sensitive Drug Delivery. Tissue Engineering Part A 2018.
37. Olthof MG, Kempen DH, Liu X, Dadsetan M, Tryfonidou MA, Yaszemski MJ, Dhert WJ, Lu L. Bone morphogenetic protein-2 release profile modulates bone formation in phosphorylated hydrogel. Journal of tissue engineering and regenerative medicine 2018;12(6):1339–1351. [PubMed: 29603878]

38. Liu X, Kim JC, Miller AL, Waletzki BE, Lu L. Electrically conductive nanocomposite hydrogels embedded with functionalized carbon nanotubes for spinal cord injury. New Journal of Chemistry 2018;42(21):17671–17681.
39. Kinard LA, Kasper FK, Mikos AG. Synthesis of oligo(poly(ethylene glycol) fumarate). Nature Protocols 2012;7(6):1219–1227. [PubMed: 22653160]
40. Liu X, Miller II AL, Park S, Waletzki BE, Terzic A, Yaszemski MJ, Lu L. Covalent crosslinking of graphene oxide and carbon nanotube into hydrogels enhances nerve cell responses. Journal of Materials Chemistry B 2016;4(43):6930–6941. [PubMed: 32263560]
41. Dadsetan M, Hefferan TE, Szatkowski JP, Mishra PK, Macura SI, Lu L, Yaszemski MJ. Effect of hydrogel porosity on marrow stromal cell phenotypic expression. Biomaterials 2008;29(14):2193–2202. [PubMed: 18262642]
42. Shi K, Wang Y-L, Qu Y, Liao J-F, Chu B-Y, Zhang H-P, Luo F, Qian Z-Y. Synthesis, characterization, and application of reversible PDLLA-PEG-PDLLA copolymer thermogels in vitro and in vivo. Scientific reports 2016;6:19077. [PubMed: 26752008]
43. Müller M, Becher J, Schnabelrauch M, Zenobi-Wong M. Nanostructured Pluronic hydrogels as bioinks for 3D bioprinting. Biofabrication 2015;7(3):035006. [PubMed: 26260872]
44. Bertassoni LE, Cardoso JC, Manoharan V, Cristino AL, Bhise NS, Araujo WA, Zorlutuna P, Vrana NE, Ghaemmaghami AM, Dokmeci MR and others. Direct-write bioprinting of cell-laden methacrylated gelatin hydrogels. Biofabrication 2014;6(2).
45. Dubbin K, Tabet A, Heilshorn SC. Quantitative criteria to benchmark new and existing bio-inks for cell compatibility. Biofabrication 2017;9(4):044102. [PubMed: 28812982]
46. Bertassoni LE, Cecconi M, Manoharan V, Nikkhah M, Hjortnaes J, Cristino AL, Barabaschi G, Demarchi D, Dokmeci MR, Yang YZ and others. Hydrogel bioprinted microchannel networks for vascularization of tissue engineering constructs. Lab on a Chip 2014;14(13):2202–2211. [PubMed: 24860845]
47. Yin J, Yan M, Wang Y, Fu J, Suo H. 3D bioprinting of low-concentration cell-laden gelatin methacrylate (GelMA) bioinks with a two-step cross-linking strategy. ACS applied materials & interfaces 2018;10(8):6849–6857. [PubMed: 29405059]
48. Guo X, Park H, Liu G, Liu W, Cao Y, Tabata Y, Kasper FK, Mikos AG. In vitro generation of an osteochondral construct using injectable hydrogel composites encapsulating rabbit marrow mesenchymal stem cells. Biomaterials 2009;30(14):2741–2752. [PubMed: 19232711]
49. Lam J, Lu S, Meretoja VV, Tabata Y, Mikos AG, Kasper FK. Generation of osteochondral tissue constructs with chondrogenically and osteogenically predifferentiated mesenchymal stem cells encapsulated in bilayered hydrogels. Acta Biomaterialia 2014;10(3):1112–1123. [PubMed: 24300948]
50. Park H, Temenoff JS, Tabata Y, Caplan AI, Raphael RM, Jansen JA, Mikos AG. Effect of dual growth factor delivery on chondrogenic differentiation of rabbit marrow mesenchymal stem cells encapsulated in injectable hydrogel composites. Journal of Biomedical Materials Research Part A 2009;88A(4):889–897.
51. Ozbolat IT, Hospodiuk M. Current advances and future perspectives in extrusion-based bioprinting. Biomaterials 2016;76:321–343. [PubMed: 26561931]
52. Shanjani Y, Pan C, Elomaa L, Yang Y. A novel bioprinting method and system for forming hybrid tissue engineering constructs. Biofabrication 2015;7(4):045008. [PubMed: 26685102]
53. Zhu W, Cui H, Boualam B, Masood F, Flynn E, Rao RD, Zhang Z-Y, Zhang LG. 3D bioprinting mesenchymal stem cell-laden construct with core–shell nanospheres for cartilage tissue engineering. Nanotechnology 2018;29(18):185101. [PubMed: 29446757]
54. Rider P, Kačarević ŽP, Alkildani S, Retnasingh S, Barbeck M. Bioprinting of tissue engineering scaffolds. Journal of tissue engineering 2018;9:2041731418802090–2041731418802090.
55. Liu W, Heinrich MA, Zhou Y, Akpek A, Hu N, Liu X, Guan X, Zhong Z, Jin X, Khademhosseini A. Extrusion bioprinting of shear-thinning gelatin methacryloyl bioinks. Advanced healthcare materials 2017;6(12):1601451.
56. Djabourov M, Leblond J, Papon P. Gelation of aqueous gelatin solutions. I. Structural investigation. Journal de physique 1988;49(2):319–332.

57. Sarker B, Singh R, Silva R, Roether JA, Kaschta J, Detsch R, Schubert DW, Cicha I, Boccaccini AR. Evaluation of Fibroblasts Adhesion and Proliferation on Alginate-Gelatin Crosslinked Hydrogel. PLOS ONE 2014;9(9):e107952. [PubMed: 25268892]

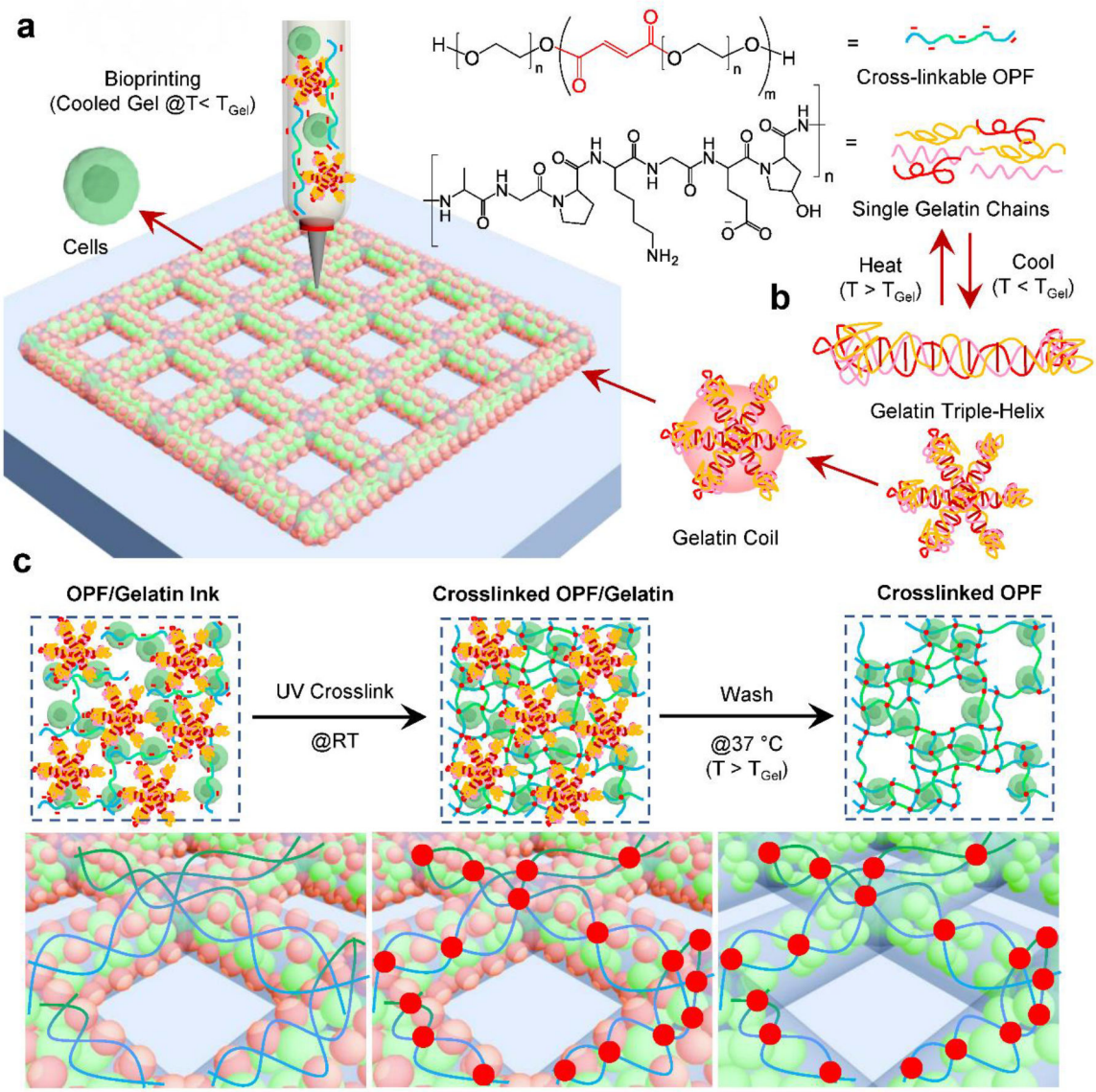

Fig. 1.

a) The schematic demonstration of the bioprinting process using photo-crosslinkable OPF polymer and gelatin chains with cells. b) Mechanism of thermos-responsive gelatin chains to form coils with reversible triple-helix. c) After bioprinting, the scaffolds were crosslinked under UV irradiation followed by the production of micro-pores through the dissolution of gelatin coils by washing in media at 37 °C.

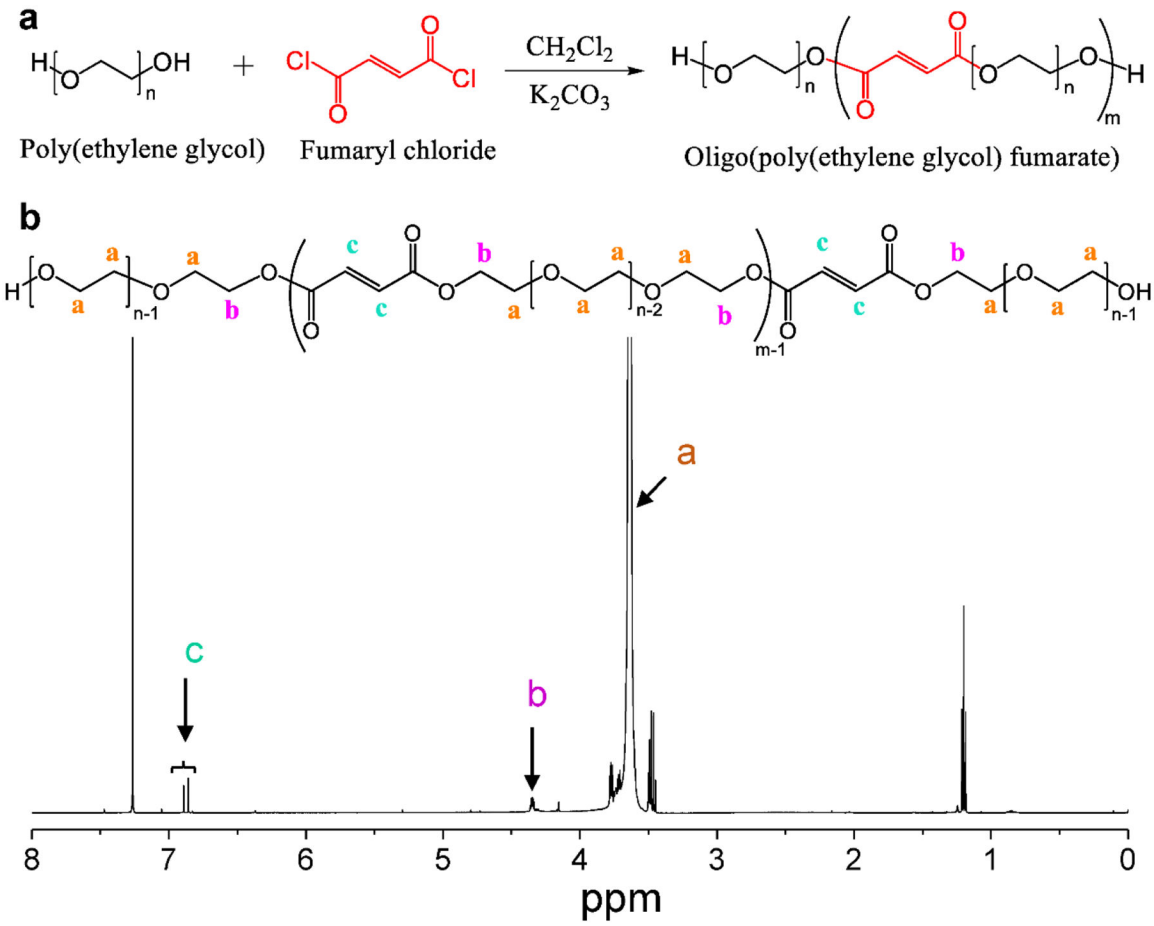

Fig. 2.

a) The synthesis route for the OPF polymer using poly(ethylene glycol) and fumaryl chloride in the presence of excess K_2CO_3 as a proton scavenger. b) The ^1H NMR spectra of the synthesized OPF polymer.

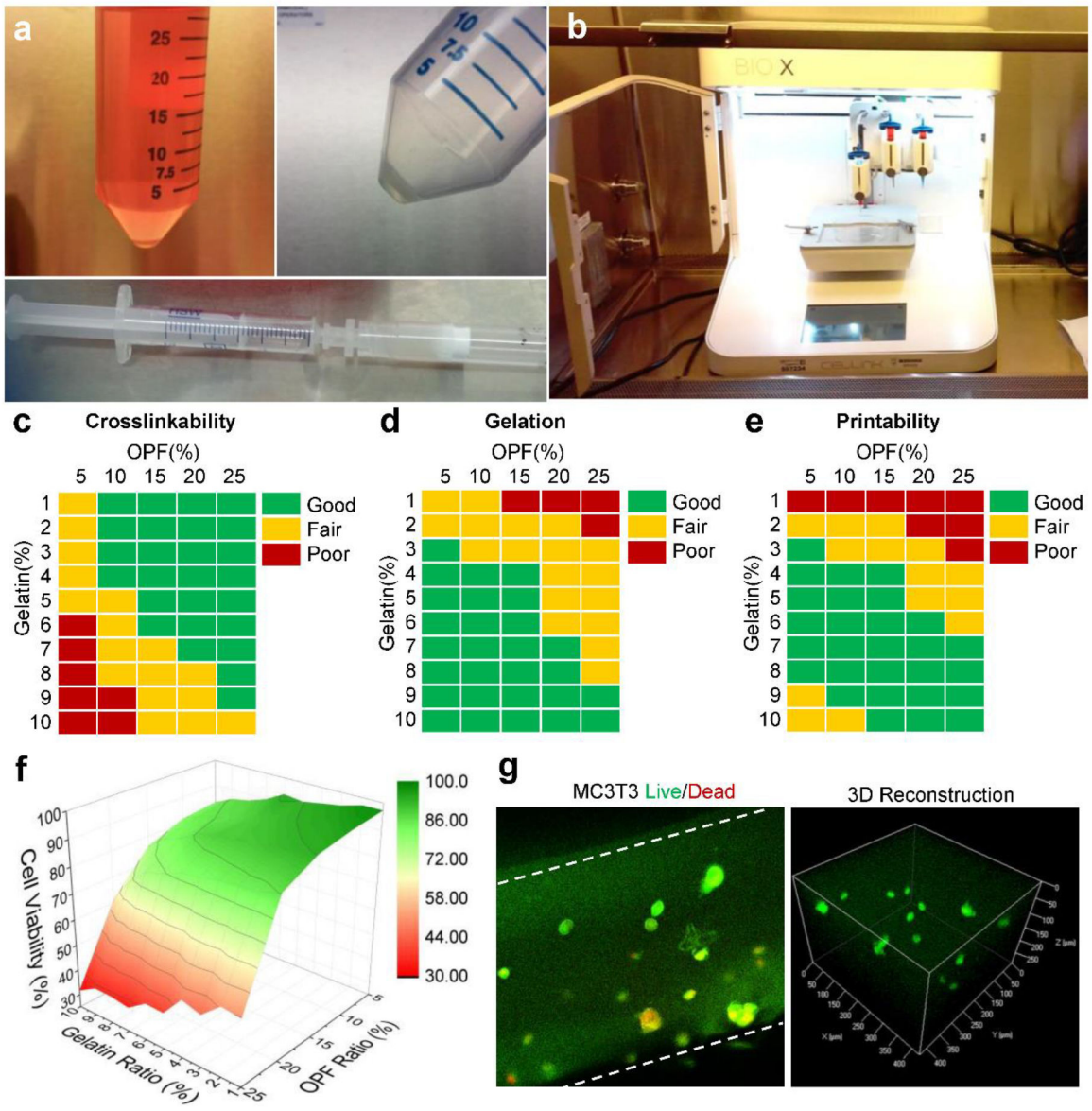

Fig. 3.

a) The collection of MC3T3 pre-osteoblast cells from the culture medium and mix with liquidized gels to obtain the bioink. b) Photographs of the bioprinting apparatus set-up using a CELLINK Bio-X printer in a sterilized cell culture hood. The c) crosslinking ability, d) gelation performance and e) printability of bioinks with varied OPF and gelatin concentrations. f) Cell viabilities of bioinks with varied OPF and gelatin concentrations. g) Confocal imaging of LIVE/DEAD stained cells encapsulated within the bioprinted scaffolds: live cells (green) and dead cells (red). Cell density: 1×10^6 cells/mL medium.

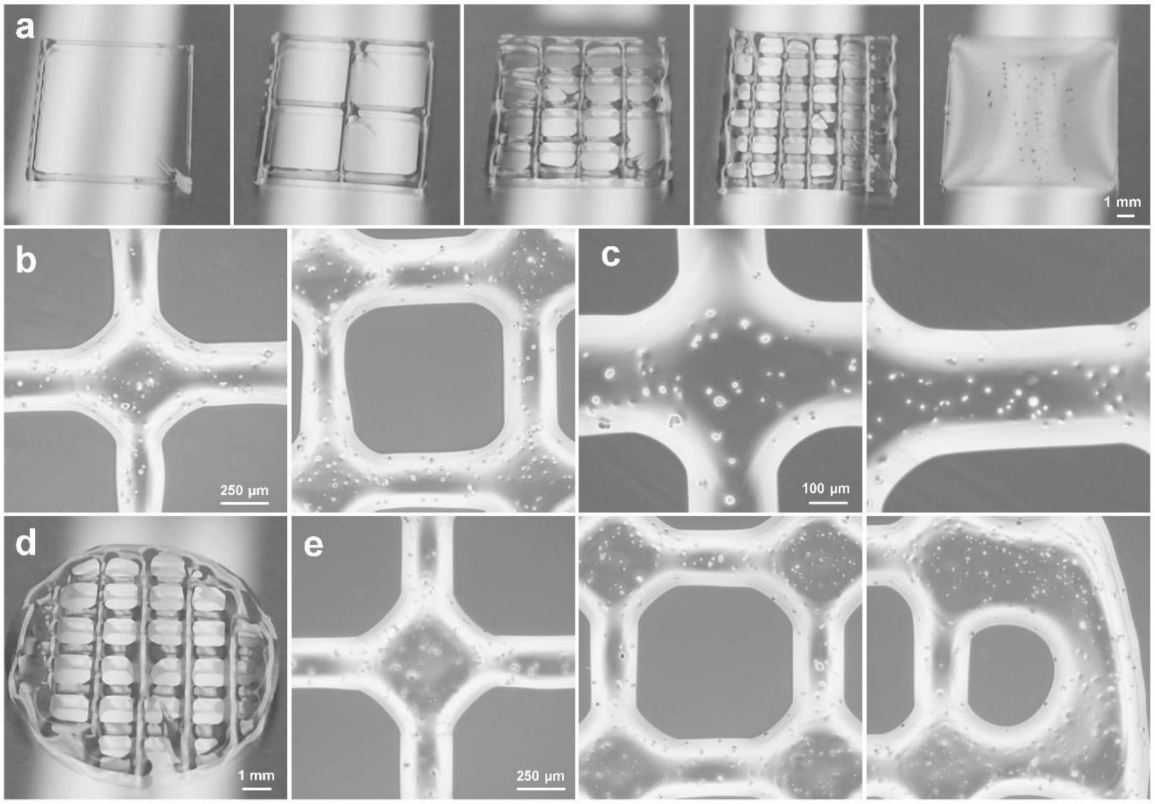

Fig. 4.

Bioprinted scaffolds morphology. a) Rectangular scaffolds printed with different infill densities. b) Microscopic images of the same printed scaffolds at different positions of the scaffolds and c) enlarged microscopic images of the scaffolds containing cells (1×10^6 cells/mL of bioink). d) Photographs of the bioprinted circular scaffolds. e) Microscopic images at different locations along the bioprinted circular scaffolds.

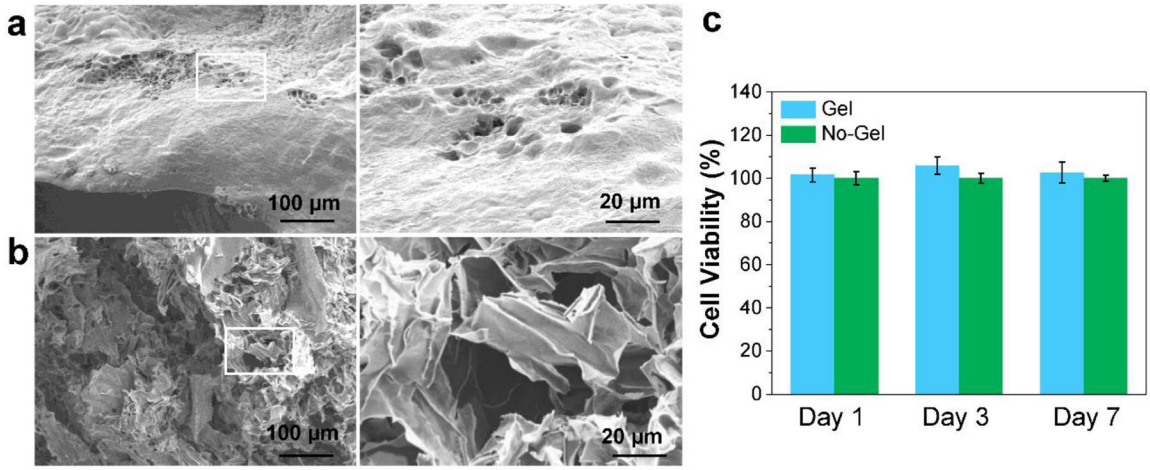

Fig. 5.

Bioink properties. SEM images of crosslinked OPF ink a) before and b) after washing. c) The MC3T3 cell viability under exposure to the leaching medium from the bioprinted scaffolds (No-Gel control was set as 100%).

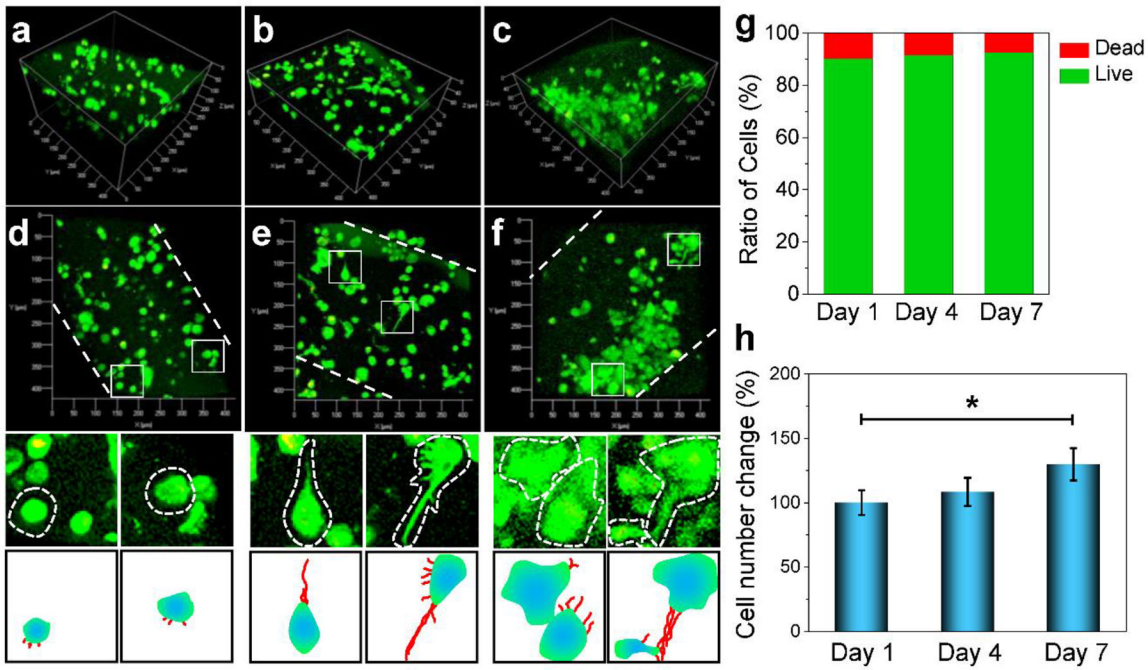

Fig. 6.

Confocal imaging. 3D imaging of the distribution of MC3T3 pre-osteoblast cells encapsulated in the bioprinted scaffolds at a) day 1, b) day 4 and c) day 7 of culture in α-MEM. 2D cell morphological features with enlarged view of single cell from the above confocal images and schematic demonstration of cell projections within the bioink at d) day 1, e) day 4 and f) day 7 of culture. g) The MC3T3 live cell and dead cell ratios. h) MC3T3 cell number changes at day 1, 4, 7 days of culture (*: $p < 0.05$).

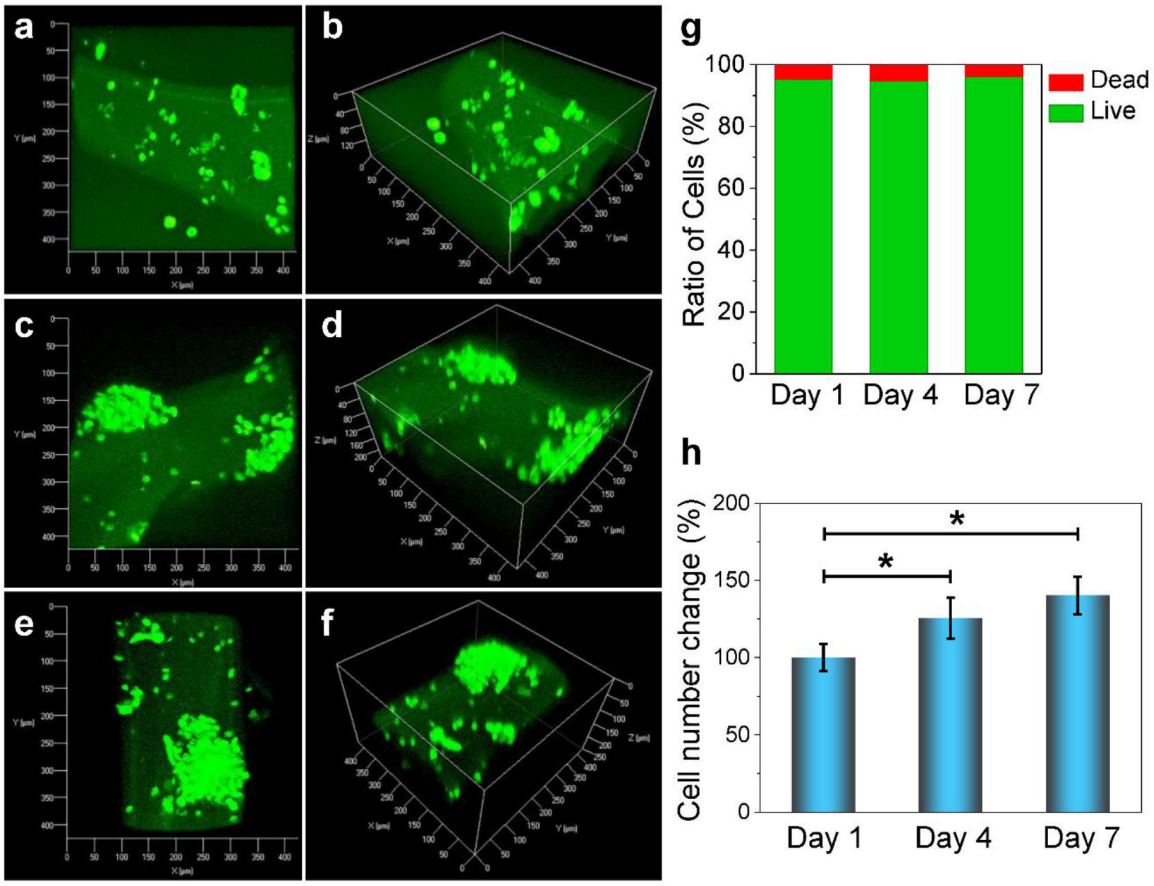

Fig. 7.

Confocal images and 3D-reconstruction images showing proliferation and morphological features of PC12 nerve cells encapsulated in bioprinted OPF scaffolds at a-b) day 1, c-d) day 4 and e-f) day 7 post-printing. g) The PC12 live cell and dead cell ratios. h) PC12 cell number changes at day 1, 4, 7 days of culture (*: $p < 0.05$).